

## Highly efficient degradation of organic pollutant mixtures by a Fe(III)-based MOF-catalyzed Fenton-like process in subcritical water



Felycia Edi Soetaredjo<sup>a,b,\*</sup>, Shella Permatasari Santoso<sup>a,b</sup>, Valentino Bervia Lunardi<sup>a</sup>, Alfin Kurniawan<sup>a,c,\*</sup>, Hardy Shuwanto<sup>d</sup>, Jenni Lie<sup>b</sup>, Kuncoro Foe<sup>a</sup>, Wenny Irawaty<sup>a</sup>, Maria Yuliana<sup>a</sup>, Jindrayani Nyoo Putro<sup>a</sup>, Artik Elisa Angkawijaya<sup>e</sup>, Yi-Hsu Ju<sup>e</sup>, Suryadi Ismadji<sup>a,b</sup>

<sup>a</sup> Department of Chemical Engineering, Widya Mandala Surabaya Catholic University, Kalijudan 37, Surabaya 60114, Indonesia

<sup>b</sup> Department of Chemical Engineering, National Taiwan University of Science and Technology, No. 43, Sec. 4, Keelung Road, Taipei 10607, Taiwan

<sup>c</sup> Department of Chemistry, National Sun Yat-Sen University, Kaohsiung 80424, Taiwan

<sup>d</sup> Department of Materials Science and Engineering, National Taiwan University of Science and Technology, No. 43, Sec. 4, Keelung Road, Taipei 10607, Taiwan

<sup>e</sup> Graduate Institute of Applied Science, National Taiwan University of Science and Technology, No. 43, Sec. 4, Keelung Road, Taipei 10607, Taiwan

### ARTICLE INFO

#### Article history:

Received 7 July 2021

Revised 25 October 2021

Accepted 26 October 2021

Available online 30 October 2021

#### Keywords:

Fenton-like process

Photoresist solvent

Monoaromatic compounds

Subcritical water

Hydroxyl radicals

Breathing MOF

### ABSTRACT

Propylene glycol monomethyl ether acetate (PGMEA) photoresist solvent and monoaromatics are typical organic pollutants found in the wastewater discharged from semiconductor manufacturing processes. Conventional treatment technologies, however, remain mostly ineffective to eliminate these pollutants from aqueous streams. Herein, we developed a novel strategy for highly efficient degradation of PGMEA and archetypal monoaromatics (i.e., benzene, toluene, xylene, phenol, and cresol) in aqueous solution by heterogeneous Fenton-like process with a flexible Fe-MOF (MIL-88B) under mild subcritical water (SCW) condition (100 °C). The as-synthesized MIL-88B(Fe) microbipyramids possess large pore channels (~32 nm) and open iron sites. The results showed that the SCW-mediated heterogeneous Fenton-like process at 100 °C with an optimal catalyst loading of 1 wt% exhibited a remarkable degradation performance toward target organic pollutants in a multicomponent system, affording a 92% total organic carbon (TOC) removal in 60 min. This mineralization efficiency was found to be notably superior to those of traditional homogeneous Fenton (FeSO<sub>4</sub>/H<sub>2</sub>O<sub>2</sub>; ~54%) and Fenton-SCW (~60%) processes. The practicability of this approach was demonstrated using real world water samples (i.e., river water, fishpond water, and wastewater) with >80% TOC removal efficiency. This study showed that the heterogeneous Fenton-like process utilizing an inexpensive, nontoxic, and reusable MIL-88B(Fe) MOF under mild SCW conditions is a promising strategy for treating semiconductor waste effluents and environmental water matrices containing toxic recalcitrant organics in an eco-friendly and efficient manner.

© 2021 Elsevier B.V. All rights reserved.

### 1. Introduction

Semiconductor manufacturing industries have been a leading figure in the development of advanced microchips that power many portable consumer electronics, such as smartphones, laptops, tablets, and other wearable computing devices. Over the coming half-decade, the global semiconductor market is projected to grow with a compound annual growth rate (CAGR) of 3.4% [37], driven by greater demand for advanced consumer and automotive electronics platforms, alongside the emerging digital technologies

including artificial intelligence, 5G, and the Internet of Things. Despite its crucial importance to modern electronics, the discharge of wastewater effluents from semiconductor processing operations to freshwater ecosystems poses significant concerns to human health and the environment. In this regard, semiconductor manufacturing effluents typically consist of a complex mixture of organic solvents, heavy metals, acids, bases, additives, and other compounds that are generated during the surface cleaning and rinsing operations [4,16,15,56]. Among those organic solvents, propylene glycol monomethyl ether acetate (PGMEA) is routinely used as the carrier solvent in the photoresist processing of semiconductor chips, due to its excellent thermal stability, biodegradability, low surface tension, and high miscibility with water and most organic solvents [47,53]. Despite its low bioconcentration potential and systemic toxicity toward aquatic organisms [40],

\* Corresponding authors at: Department of Chemical Engineering, Widya Mandala Surabaya Catholic University, Kalijudan 37, Surabaya 60114, Indonesia.

E-mail addresses: [felyciae@yahoo.com](mailto:felyciae@yahoo.com) (F.E. Soetaredjo), [alfin\\_kur@yahoo.com](mailto:alfin_kur@yahoo.com) (A. Kurniawan).

the release of large amounts of PGMEA and its degradation products into the environment may still pose a threat to both human health and the environment. For instance, the repeated exposures of PGMEA to animals and humans via dietary or inhalation can cause depression of the central nervous system and induces hepatic dysfunction [6] (Huang and Wu, 2019), as well as some disorders in the kidney and renal systems for the chronic effect (Huang and Wu, 2019). In addition, the photochemical and thermal decomposition of photoresists during the photolithographic process can generate toxic and carcinogenic aromatic compounds, such as benzene, toluene, xylene, phenol, and cresol (Huang and Wu 2009) [32]. The presence of these monoaromatic pollutants in water bodies (even at low concentration levels) has been associated with numerous adverse health effects on the aquatic species and humans [28]. Due to the relatively high water solubility of PGMEA (160 g/L [40]) and monoaromatic compounds, these organic pollutants are likely to be present in semiconductor effluents and can persist in aquatic environments at high concentrations if left without remediation.

Conventional technologies to remove PGMEA and archetypal monoaromatic compounds from water and wastewater, such as coagulation-precipitation, bioremediation, and membrane processes have several disadvantages including low removal efficiency, energy intensive, and the production of large quantities of toxic chemical sludge. On the other hand, the advanced oxidation processes (AOPs) based on Fenton and Fenton-like reactions have shown great promise in the degradation of toxic and refractory contaminants in aqueous waste streams [3,9,39,54] (Yu et al., 2014). The central importance of Fenton and Fenton-like AOPs lies in the efficient generation of highly reactive and strongly oxidizing hydroxyl radicals ( $\text{HO}\cdot$ ) from the decomposition of hydrogen peroxide ( $\text{H}_2\text{O}_2$ ) mediated by transition metal ions (most notably  $\text{Fe}^{2+}$  and  $\text{Cu}^+$ ) or solid catalysts. In recent years, numerous heterogeneous Fenton-like catalysts, ranging from iron oxychloride [51] and supported single Fe atoms [52] to hybrid nanocomposites [24,29,50], have been investigated with respect to their activity and durability toward  $\text{H}_2\text{O}_2$  activation to generate  $\text{HO}\cdot$  radicals. Iron-based metal-organic frameworks (Fe-MOFs) are promising platforms for promoting Fenton-like and other catalytic reactions [10,22,42,45,46], due to their high internal surface areas and porosity, excellent visible light absorption, robust thermal and chemical stability, and inexpensive, nontoxic, and earth-abundant metal source. In addition to these unique characteristics, the abundant and well-distributed metal centers within the porous framework, alongside open pore channels may afford significant benefit for the adsorption of guest species and subsequent reactions on these catalytic active sites with none-to-little mass transport limitations, thus presenting an unique attribute from which most traditional rigid porous catalysts suffer.

While there have been several reports of Fe-based MOFs as catalysts for Fenton-like catalytic oxidation of aqueous pollutants, most of these studies are limited to the degradation of organic dyes and other simple molecules in the single component system (see SI, Table S1). In fact, study of the MOF-catalyzed Fenton-like degradation of organic pollutants in multicomponent aqueous mixtures, which are the more typical scenario in real-world environments, remains so far unexplored. In this study, we demonstrated for the first time that the heterogeneous Fenton-like process using a flexible MIL-88B(Fe) microcrystals (MIL stands for Materials from Institut Lavoisier) in subcritical water (SCW) can lead to a highly efficient degradation of PGMEA and monoaromatic compounds (i.e., benzene, toluene, xylene, phenol, and cresol) from their aqueous mixtures, leading to an outstanding TOC removal efficiency of >90% within 60 min treatment. The widely tunable physical properties of SCW have enabled its utilization as an environmentally benign solvent and acid/base bifunctional catalyst in many

applications, such as waste and biomass valorization [18,19], chemical reduction of nitroarene [41], and size-controlled synthesis of nanoparticles [31]. However, its intriguing role in the Fenton-like catalytic oxidation remains largely unexplored. In this context, the unique properties of SCW medium to solubilize nonpolar organic molecules and produce higher amounts of hydronium ( $\text{H}_3\text{O}^+$ ) and hydroxide ions ( $\text{OH}^-$ ) in the combination of Fenton-like reaction system for the enhanced production of  $\text{HO}\cdot$  radicals. To the best of our knowledge, there has been no available study in the literature demonstrating highly efficient degradation of organic pollutant mixtures associated with semiconductor manufacturing discharge using a Fenton-like process with an iron-based breathing MOF under mild SCW conditions. Moreover, the practicability of this approach was demonstrated for the degradation of target organic pollutants from real world water samples. Furthermore, the kinetic and thermodynamic activation parameters of Fenton and Fenton-like reactions in SCW, along with the degradation mechanism of model organic pollutants on the surface of MIL-88B(Fe) are evaluated.

## 2. Experimental

### 2.1. Materials

Iron(II) sulfate heptahydrate ( $\text{FeSO}_4 \cdot 7\text{H}_2\text{O}$ , ACS reagent,  $\geq 99\%$ ), iron(III) chloride hexahydrate ( $\text{FeCl}_3 \cdot 6\text{H}_2\text{O}$ , ACS reagent, 97%),  $\text{H}_2\text{O}_2$  solution (30 wt% in  $\text{H}_2\text{O}$ ), terephthalic acid (TPA,  $\text{C}_6\text{H}_4(\text{COOH})_2$ , 98%), PGMEA ( $\text{C}_6\text{H}_{12}\text{O}_3$ , ReagentPlus,  $\geq 99.5\%$ ), benzene ( $\text{C}_6\text{H}_6$ , ACS reagent,  $\geq 99\%$ ), toluene ( $\text{C}_6\text{H}_5\text{CH}_3$ , anhydrous, 99.8%), *o*-xylene ( $\text{C}_6\text{H}_4(\text{CH}_3)_2$ , anhydrous, 97%), phenol ( $\text{C}_6\text{H}_5\text{OH}$ ,  $\geq 99\%$ ), *p*-cresol ( $\text{CH}_3\text{C}_6\text{H}_4\text{OH}$ , 99%), ethanol ( $\text{C}_2\text{H}_5\text{OH}$ , HPLC grade,  $\geq 99.8\%$ ), and *N,N*-dimethylformamide (DMF, HPLC grade, 99%) were purchased from Sigma-Aldrich and used as received without additional treatment. Deionized (DI) water with a  $18.2 \text{ M}\Omega \text{ cm}^{-1}$  specific resistivity was produced from a Millipore water purification system.

### 2.2. Solvothermal synthesis of MIL-88B(Fe) and materials characterization

The MIL-88B(Fe)[DMF] was solvothermally synthesized following the reported procedure by Horcajada et al. [14], but without the addition of base.  $\text{FeCl}_3 \cdot 6\text{H}_2\text{O}$  (2.7 g, 10 mmol) and TPA (1.66 g, 10 mmol) were dissolved in DMF (50 mL) under magnetic stirring and the resultant mixture was transferred into a 100 mL Teflon-lined stainless steel autoclave. The molar ratio of metal:ligand:solvent in the reaction mixture was 1:1:646. The sealed vessel was then heated at  $150^\circ\text{C}$  overnight in an oven under static conditions. Afterward, the autoclave was left to cool to room temperature and the resulting precipitate was collected via vacuum filtration, followed by a multiple washing step with DI water and ethanol to remove unreacted precursors and DMF solvent molecules from the pores. The washed powders were dried in an oven at  $80^\circ\text{C}$  for at least 2 h to afford an orange MIL-88B(Fe) solid.

Textural characteristics of the as-synthesized MIL-88B(Fe) were examined by nitrogen physisorption isotherms at 77 K, on a Micromeritics ASAP 2010 volumetric sorption analyzer. Prior to sorption measurements, the sample was degassed under vacuum at  $150^\circ\text{C}$  for 12 h. The specific surface area was determined from the adsorption branch of the isotherm using the standard Brunauer-Emmett-Teller (BET) method applied in the relative pressure range ( $P/P_0$ ) from 0.05 to 0.3. The pore size distribution (PSD) was analyzed by the Barrett-Joyner-Halenda theory (BJH) model applied to the desorption isotherm. Powder X-ray diffraction (PXRD) pattern was collected at room

temperature using a Bruker D2 Phaser tabletop diffractometer equipped with a Cu K $\alpha$  X-ray source (40 kV and 30 mA). Fourier transform infrared (FTIR) spectra were collected on a JASCO FT/IR 4100 spectrometer over the 4000–400 cm<sup>-1</sup> region using the KBr pellet method. The morphology of the sample was examined using a FEI Inspect F50 field-emission scanning electron microscope (SEM) operating at 10 kV.

### 2.3. SCW-mediated Fenton and Fenton-like degradation experiments

The catalytic performance of MIL-88B(Fe) was tested in the Fenton-like degradation of PGMEA and several benzene derived compounds under mild SCW conditions. An aqueous mixture comprising PGMEA (500 mg L<sup>-1</sup>), benzene (250 mg L<sup>-1</sup>), toluene (250 mg L<sup>-1</sup>), *o*-xylene (250 mg L<sup>-1</sup>), phenol (250 mg L<sup>-1</sup>), and cresol (250 mg L<sup>-1</sup>) was employed as the model semiconductor wastewater. Note here that the concentrations of all model pollutants are well below their water solubility limits except for the *o*-xylene (see SI, Table S2), thus ensuring the single-phase system. The pH of the synthetic wastewater solution was adjusted to  $\sim$ 3 using an aqueous H<sub>2</sub>SO<sub>4</sub> solution. In a typical experiment, the synthetic wastewater solution (100 mL) and a certain amount of catalyst powder (0.5–1.5 wt%) were mixed in a 150 mL borosilicate glass vial and stirred for 30 min to establish the adsorption–desorption equilibrium. The mixture was subsequently placed in a high-pressure stainless steel batch reactor equipped with Swagelok tube fittings and tightly sealed with its closure head by M8 screws. The details of the reactor setup can be found elsewhere [11,19]. The reactor was initially pressurized to 300 psi with O<sub>2</sub> (99.9995% purity) to maintain the liquid phase condition during the process. Subsequently, the reactor was heated to the target temperatures (i.e., 100, 120, 160, 200, and 240 °C) and held for 5 min to ensure a stable temperature. Then, 0.2 mL of H<sub>2</sub>O<sub>2</sub> solution (30%) was fed into the reactor and the reaction was maintained for 60, 90, and 120 min. After a predetermined reaction time, the heating element was turned off and the reaction was subsequently quenched by immersion in a water bath. The catalyst powder was collected by filtration, washed with ethanol and water several times, and dried in an oven for further analysis. The concentrations of total organic carbon (TOC) in the initial and treated wastewater solutions were measured using a Shimadzu TOC-L analyzer. Homogeneous Fenton-SCW degradation experiments were performed under the same reaction conditions using conventional Fenton reagent (1 mL) composed of FeSO<sub>4</sub>·7H<sub>2</sub>O (0.139 g, 0.5 mmol), H<sub>2</sub>O<sub>2</sub> (0.6 mL), and DI water (9.4 mL). Note that the Fenton reagent solution was freshly prepared each time just before the system temperature reached a stable state and then quickly introduced into the reactor. Control experiments were also conducted without the addition of iron source and H<sub>2</sub>O<sub>2</sub> to evaluate the extent of mineralization of PGMEA and model monoaromatic compounds under the SCW conditions.

## 3. Results and discussions

### 3.1. Characterizations of MIL-88B(Fe)

MIL-88B(Fe), which has a chemical formula of Fe<sub>3</sub>O[O<sub>2</sub>C-C<sub>6</sub>H<sub>4</sub>-CO<sub>2</sub>]<sub>3</sub>X·*n*H<sub>2</sub>O (X = Cl, OH), represents an archetypal metal terephthalate MOF with dynamic pore structure that readily undergoes an extensive and reversible structural swelling without losing either porosity or crystalline order upon the introduction of guest molecules [14,38]. In the liquid-phase adsorption, such the framework breathing behavior plays a crucial role in modulating both the adsorption capacity and selectivity toward a particular adsorbate through specific guest–framework and guest–guest interac-

tions. In addition, the enhancement of the catalytic activity of flexible MIL-type MOF structures can be realized through the expansion of the unit cell volume, which allows more efficient transport of the reactant molecules to the catalytic sites. For example, Gao and co-workers (2013) reported higher Fenton-like catalytic activity of flexible MIL-88B(Fe) than the rigid MIL-101(Fe) for phenol degradation, which could be attributed to the greater accessibility of coordinatively unsaturated iron sites to H<sub>2</sub>O<sub>2</sub> molecules. Nivetha et al. [30] showed that the hydrated MIL-53(Fe) with an enlarged pore size and higher BET surface area exhibits superior catalytic performance toward electrocatalytic H<sub>2</sub> evolution and visible light photodegradation, implying that the MIL-53(Fe) with an open pore structure is required for the enhanced performance in adsorption and catalysis.

The N<sub>2</sub> adsorption–desorption curves at 77 K of the as-synthesized MIL-88B(Fe) are shown in Fig. 1a, which resemble a type II isotherm shape following IUPAC classification [43]. As can be seen in the isotherm curve, the insignificant N<sub>2</sub> uptake at low relative pressure ( $P/P_0 < 0.01$ ), together with the absence of an inflection point at  $P/P_0 \sim 0.1$  indicates the restricted adsorption of N<sub>2</sub> molecules in very narrow micropores, in agreement with the closed pore configuration of the dehydrated MIL-88B(Fe) after activation by vacuum degassing [14,38]. The gradual rise of the isotherm curve over the range  $0.05 < P/P_0 < 0.8$  could be attributed to the multilayer adsorption in small mesopores. Furthermore, a significant N<sub>2</sub> uptake without reaching the saturation point at high  $P/P_0$  (0.8–1.0), along with the inflection “knee” at 0.45–0.50  $P/P_0$  in the desorption curve, suggests the existence of large mesopores and/or macropores within the MIL-88B(Fe) structure [35]. The predominant mesoporous nature of the as-synthesized MOF material is further confirmed by the BJH PSD curve (Fig. 1a, inset), which reveals a bimodal pore size distribution centered at 3.8 and 32.5 nm. The BET specific surface area and total pore volume (measured at  $P/P_0$  0.994) of the MIL-88B(Fe) are calculated to be 22.1 m<sup>2</sup> g<sup>-1</sup> and 0.08 cm<sup>3</sup> g<sup>-1</sup>, respectively, which correspond well with literature reported values for dry closed pore form of this material [14].

The PXRD pattern of the resultant MIL-88B(Fe) is depicted in Fig. 1b, showing the highly crystalline nature of the sample. An excellent match in the Bragg reflection positions between the experimental and simulation from the single crystal data [25] implies the successful formation of the MIL-88B(Fe) phase in the MOF product. The intense Bragg reflections located at  $2\theta = 9.69^\circ$ ,  $12.86^\circ$ ,  $19.11^\circ$ ,  $22.23^\circ$ , and  $28.17^\circ$  can be assigned to the lattice spacings of the hexagonal space group ( $P6_2c$ ) of MIL-88B(Fe), which is in good agreement with previous studies [25,38].

The SEM images of MIL-88B(Fe) microcrystals are displayed in Fig. 1c. As can be seen in this figure, the resultant MOF material exhibits a truncated octahedral bipyramidal morphology with well-defined edges, tips, and a relatively smooth surface. The aspect ratio (i.e., length-to-width) of the resultant MIL-88B(Fe) bipyramids is calculated to be  $1.92 \pm 0.11$ , while the measured particle sizes range between 5 and 9  $\mu$ m in length, showing a quite monodisperse size distribution (Fig. 1d). The corresponding energy dispersive X-ray spectroscopic (EDS) analysis of MIL-88B(Fe) bipyramidal microcrystals (Fig. 1c right side and Figure S1) confirmed the presence of Fe, O, and C elements, along with a small quantity of chloride (3.3 at%) as the coordinating counterion in the octahedral iron trimer. The successful formation of MIL-88B(Fe) was also evidenced by FTIR spectroscopy (see SI, Figure S2), showing the vibrational features of asymmetric ( $\nu_{as}$ ) and symmetric ( $\nu_s$ ) COO stretching modes at 1600 and 1392 cm<sup>-1</sup>, respectively and the Fe–O stretching vibration of FeO<sub>6</sub> octahedra at 548 cm<sup>-1</sup>. These assignments are in good agreement with the literature data [12].

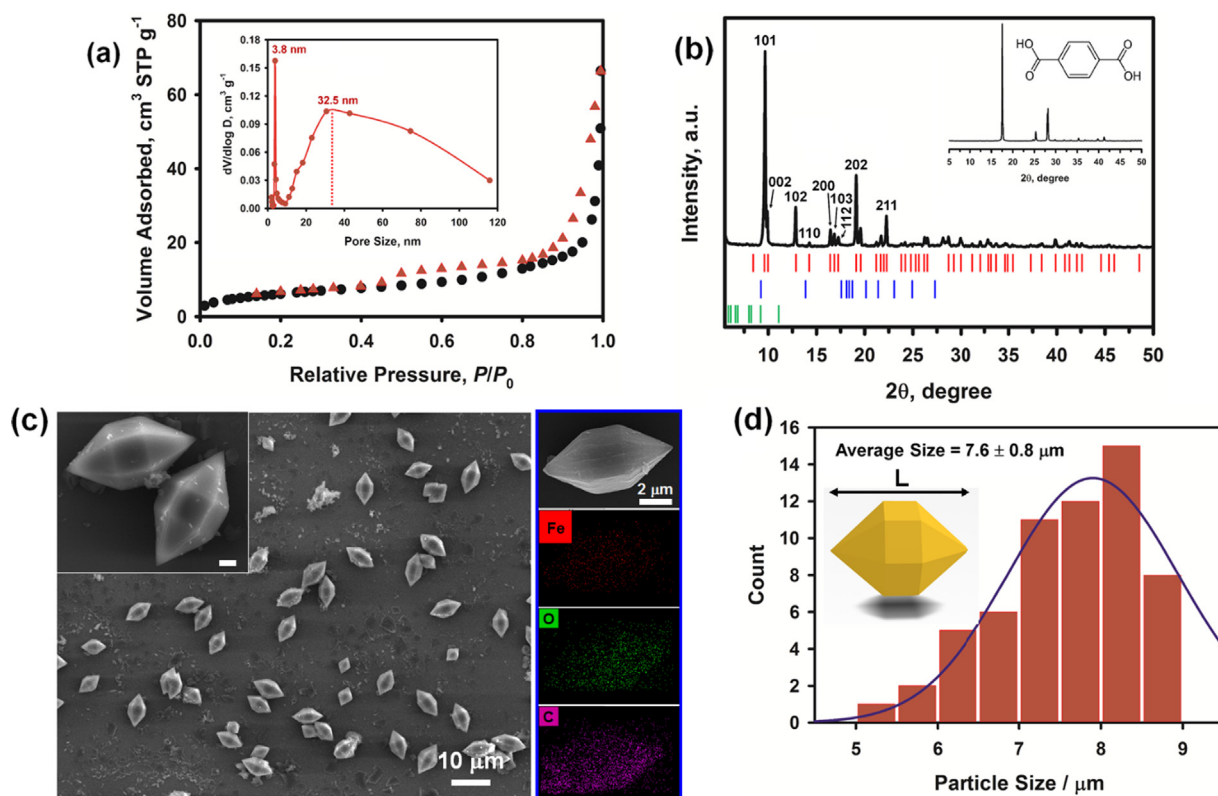


**Fig. 1.** Characterizations of the as-synthesized MIL-88B(Fe) MOF. (a) Nitrogen adsorption (black circles) and desorption (red triangles) isotherms measured at 77 K and the corresponding BJH pore size distribution curve from the desorption isotherm (inset). (b) Experimental PXRD pattern and comparison with the positions of the Bragg reflections in the calculated patterns, where red, blue, and green tick marks represent MIL-88B(Fe), MIL-53(Fe), and MIL-101(Fe) phases, respectively. Inset: XRD pattern of ditopic TPA linker. (c) SEM image of MIL-88B(Fe) bipyramids and the inset shows a magnified view of individual particles (scale bar: 1 μm). Right: the corresponding EDS elemental maps of Fe, O, and C. (d) histogram showing the size distribution of MIL-88B(Fe) bipyramidal particles determined from Fiji-ImageJ software. Inset is the corresponding geometric model. The measured particle size ( $7.6 \pm 0.8 \mu\text{m}$ ) corresponds to the average length (L) of bipyramids and the solid blue line represents the best fit with a Gaussian model ( $R^2 = 0.96$ ).

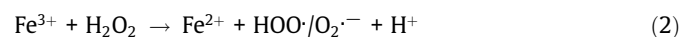
### 3.2. Catalytic degradation performance

#### 3.2.1. Conventional Fenton process

The conventional Fenton reaction between  $\text{Fe}^{2+}$  and  $\text{H}_2\text{O}_2$  remains one of the most important catalytic oxidation reactions in AOPs, due to its universal applicability to eliminate various toxic recalcitrant organic substances in a simple and efficient manner. To achieve maximum degradation efficiency, a set of operating parameters needs to be carefully considered, such as pH condition, the concentrations of Fenton's reagent ( $\text{Fe}^{2+}$  and  $\text{H}_2\text{O}_2$ ) and dissolved oxygen, and temperature [8] (Zazo et al., 2011). The adjusted pH of the synthetic wastewater solution was adjusted to 3 where maximum  $\text{HO}^\cdot$  radical formation occurred [51] and the reaction was performed under aerial  $\text{O}_2$  saturation conditions. In addition, low pH conditions also mimic the actual condition of semiconductor wastewater [2].

The treatment performance of conventional Fenton process at various temperatures toward oxidative degradation of PGMEA and model monoaromatic compounds, as measured in terms of TOC removal, is presented in Fig. 2a. The results demonstrate that the TOC removal rate is fairly rapid over the first 60 min, after which it slows down and eventually plateaued after 120 min, regardless of the reaction temperature. Within 60 min, the TOC removal efficiency reached 54.7%, 60.4%, and 62.3% at 30, 35, and 40 °C, respectively. Further prolonging the reaction time to 120 min led to only a marginal increase in the TOC removal to 62.3%, 66.9%, and 68.9%. This two-stage degradation behavior implies that the formation of  $\text{HO}^\cdot$  radicals from catalytic decomposition of  $\text{H}_2\text{O}_2$  (ferrous step, see Eq. (1)) predominant takes place

within 60 min until both the  $\text{Fe}^{2+}$  and  $\text{H}_2\text{O}_2$  concentrations in the solution became depleted, thus retarding the  $\text{HO}^\cdot$  generation rate. In the second stage, the degradation rate is mainly governed by the regeneration of  $\text{Fe}^{2+}$  from  $\text{Fe}^{3+}$  (Eq. (2)), which proved to be a much slower reaction with a second-order rate constant 4 orders of magnitude smaller than that of kinetically fast ferrous step (Duesterberg and Mylon, 2008).



The first- and second-order kinetic models are employed to describe the TOC removal kinetics of the Fenton process, as shown in Figure S3. Judged by the  $R^2$  values, the second-order model provides a better fit of the kinetic data, where the rate constant ( $k_2$ ) increases from  $1.4 \times 10^{-2} \text{ M}^{-1} \text{ min}^{-1}$  at 30 °C to  $2.3 \times 10^{-2} \text{ M}^{-1} \text{ min}^{-1}$  at 40 °C (see SI, Table S3). This result demonstrates that the formation of  $\text{HO}^\cdot$  radicals from Fe(II)-catalyzed decomposition of  $\text{H}_2\text{O}_2$  is more favorable at elevated temperatures, indicating the endothermic nature of the reaction.

#### 3.2.2. Fenton-SCW system

To date, a comprehensive study on the degradation of organic pollutants by Fenton reaction under SCW conditions remains very scarce. In the present study, the mild SCW reaction environments are generated at 100, 120, 160, 200, and 240 °C under an initial 300 psi  $\text{O}_2$  to maintain the liquid state of hot water throughout the reaction. As shown in Figure S4a, the degradation efficiency

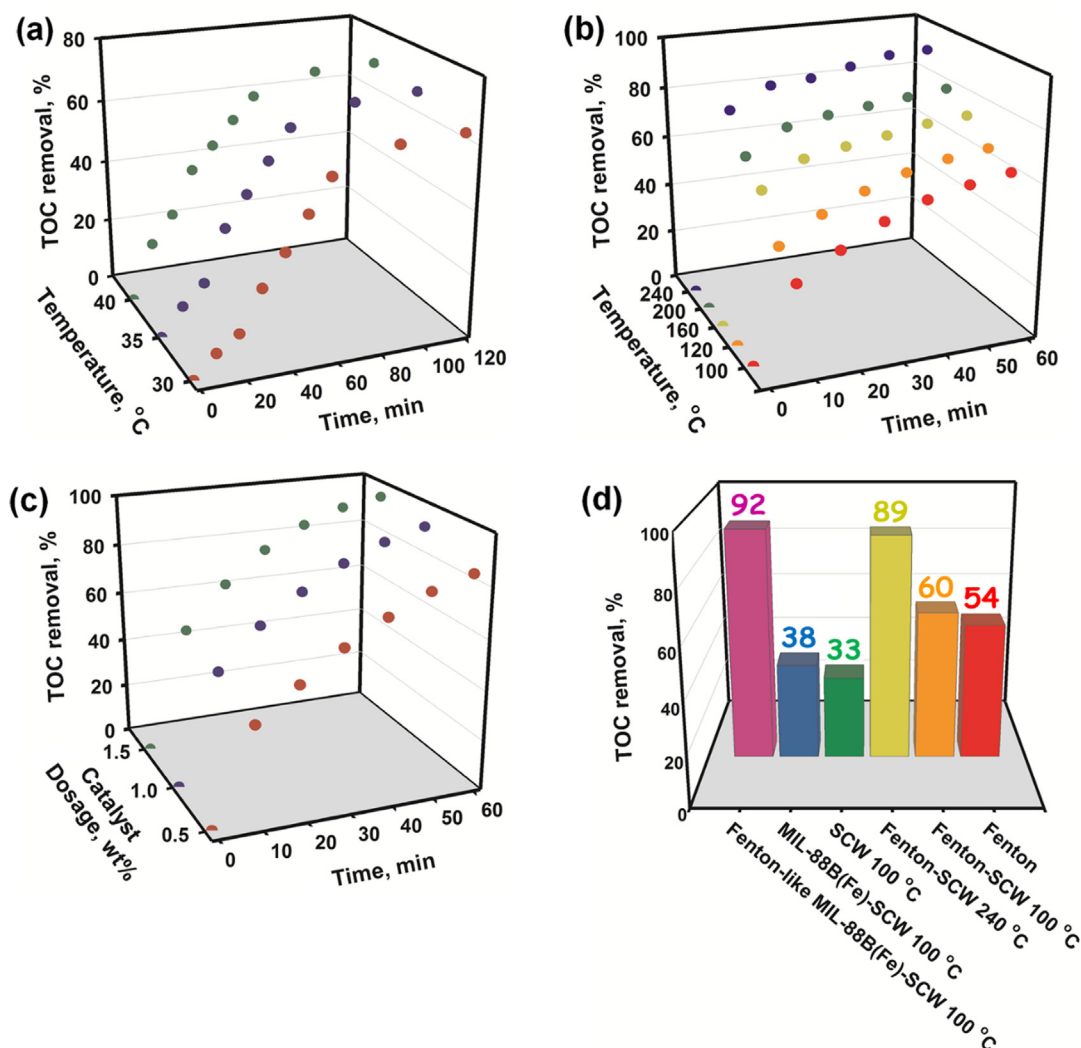


**Fig. 2.** Kinetic profiles of the TOC removal in the synthetic wastewater solution at pH 3 by (a) conventional homogeneous Fenton, (b) homogeneous Fenton-SCW, and (c) heterogeneous Fenton-like process with MIL-88B(Fe) at a SCW temperature of 100 °C. The corresponding 2D kinetic data plots are presented in Figures S3 and S5. (d) Performance comparison of Fenton-based processes investigated in this study in terms of the TOC removal efficiency for a 60 min treatment. The concentrations of the  $\text{Fe}^{2+}$  and  $\text{H}_2\text{O}_2$  in the homogeneous Fenton and Fenton-SCW processes are 500  $\mu\text{M}$  and 5.88 mM, respectively. The synthetic wastewater solution consists of PGMEA ( $C_0 = 500 \text{ mg L}^{-1}$ ) and monoaromatic compounds (i.e., benzene, toluene, *o*-xylene, phenol, and cresol;  $C_0 = 250 \text{ mg L}^{-1}$ ).

of PGMEA and monoaromatics in the synthetic wastewater solution was <60% after SCW treatment at 240 °C for 1 h. This mineralization efficiency was found to be comparable to that of conventional Fenton reaction performed at ambient temperature for 2 h (see the red spheres in Fig. 2a), thus suggesting the potential of SCW as a green and sustainable medium for the degradation of recalcitrant organic pollutants. The addition of Fenton's reagent (500  $\mu\text{M}$   $\text{Fe}^{2+}$  and 5.88 mM  $\text{H}_2\text{O}_2$ ) into the greatly enhances the degradation efficiency with nearly 90% reduction in TOC after 60 min. As shown in Figure S4b, longer treatment times of 90 and 120 min afford only a slight enhancement (<5%) in the TOC removal. Thus, 60 min was considered the optimal treatment time for the SCW-mediated homogeneous Fenton and heterogeneous Fenton-like degradation systems in this work.

The TOC removal profiles of homogeneous Fenton-SCW system (Fig. 2b) exhibits a distinctly different time-dependent behavior from low temperature Fenton process shown in Fig. 2a. In the former case, the TOC reduction proceeds rapidly within the first 10 min of the reaction, affording TOC removal efficiencies of 52.4%, 60.1%, and 73.4% at 160, 200, and 240 °C, respectively. However, after 10 min of treatment, the TOC removal rate increased

slowly until reaching a plateau around 50–60 min. These results indicate that the Fenton oxidation process, i.e., the ferrous step (Eq. (1)) takes place the dominant at early reaction times before leveling off due to the consumption of  $\text{Fe}^{2+}$  and  $\text{H}_2\text{O}_2$ . The kinetic fitting results of the first-order, second-order, and the Behnjady-Modirshahla-Ghanbary (BMG) models [5] toward the TOC removal kinetics are presented in Figure S5. As shown in this figure, the TOC removal profiles of Fenton-SCW at various temperatures do not follow first-order kinetics, as reflected by a poor fit quality with  $R^2$  values of 0.702–0.896 (Table 1). On the other hand, satisfactory correlation results are obtained with second-order ( $R^2 = 0.915$ –0.988) and the BMG ( $R^2 = 0.998$ –0.999) kinetic models where the latter provides the best fit to the data. From the BMG model fit, the nonlinear kinetic characteristic of the homogeneous Fenton-SCW system can be interpreted in terms of the physical meaning of the fitted parameters. The kinetic parameter  $1/m$ , which is associated with the initial removal rate [5], increases from 0.044 to 0.343  $\text{min}^{-1}$  with increasing SCW temperature from 100 to 240 °C. This suggests that the SCW temperature plays an important role in promoting the production rate of radicals, which is consistent with the observation in Fenton system. The reciprocal values

**Table 1**

Fitted kinetic parameters of the first-order, second-order, and BMG models for the TOC removal kinetics in homogeneous Fenton-SCW process at various temperatures.

Model <sup>†</sup>	Parameters <sup>†</sup>	Temperature (°C)				
		100	120	160	200	240
First-order kinetics $C_t = C_0 \exp(-k_1 t)$	$k_1$ (min <sup>-1</sup> )	0.019	0.023	0.034	0.047	0.094
	$R^2$	0.882	0.814	0.702	0.745	0.896
Second-order kinetics $1 - \frac{C_t}{C_0} = \frac{k_2 t}{1 + k_2 t}$	$k_2$ (M <sup>-1</sup> min <sup>-1</sup> )	0.030	0.038	0.068	0.099	0.214
	$R^2$	0.972	0.948	0.915	0.943	0.988
BMG $1 - \frac{C_t}{C_0} = \frac{t}{m + nt}$	$m$ (min)	22.883	14.827	6.013	4.393	2.912
	$n$	1.304	1.342	1.313	1.225	1.082
	$k_{\text{init}}$ (min <sup>-1</sup> )	0.044	0.067	0.166	0.228	0.343
	MOC <sub>cal</sub> (%) <sup>‡</sup>	76.7	74.5	76.2	81.6	92.4
	MOC <sub>exp</sub> (%) <sup>§</sup>	59.6	63.6	71.5	77.8	89.5
	$R^2$	0.998	0.998	0.999	0.999	0.999

<sup>†</sup> Obtained by nonlinear least-squares fitting using SigmaPlot program.<sup>‡</sup> Theoretical maximum oxidation capacity, which is equal to  $1/n$ .<sup>§</sup> TOC removal efficiency at 60 min.

of constant  $n$  corresponding to the theoretical maximum oxidation capacity (MOC) follow the same trend as reaction temperature increases from 160 to 240 °C. This can be explained by the increased ion product ( $K_w$ ) of water and consequently the oxidizing capacity. Moreover, the MOC<sub>cal</sub> values are in good agreement with the experimental ones, indicating the suitability of the BMG kinetic model to describe the TOC disappearance kinetics of model pollutants in the homogeneous Fenton-SCW process.

Compared to the homogeneous Fenton process at low temperatures, the enhanced degradation of model organic pollutants in SCW-mediated Fenton system can be ascribed to the following factors: (i) unimolecular dissociation of H<sub>2</sub>O<sub>2</sub> under pressurized O<sub>2</sub> atmosphere to produce HO• radicals (H<sub>2</sub>O<sub>2</sub> → 2 HO•), (ii) favorable *in situ* generation of H<sub>3</sub>O<sup>+</sup> and OH<sup>-</sup> ions, (iii) the increased solubility of model organic pollutants in the SCW, and (iv) higher intrinsic reaction rates provided by SCW environment. Since the H<sub>2</sub>O<sub>2</sub> decomposition below the critical temperature of water follows Arrhenius behavior [7], increasing the SCW temperature from 100 to 240 °C leads to a faster HO• generation rate and consequently a more efficient and higher TOC removal. In addition to the hydroxyl radical, the peroxy radicals (HOO•) could be formed via the reaction between H<sub>2</sub>O<sub>2</sub> and dissolved oxygen [2].

As mentioned in the point (ii) above, the *in situ* generation of H<sub>3</sub>O<sup>+</sup> and OH<sup>-</sup> species occurs more favorably under SCW conditions due to the weakening of the hydrogen bond network [36]. As a consequence, the density, dielectric constant, and the  $K_w$  of liquid H<sub>2</sub>O in the temperature range of 100–240 °C are lower compared to those at ambient conditions (see SI, Figure S6), in which the first two properties contribute to the greater solubilizing power toward organic compounds (point (iii)). With regard to point (ii), the *in situ* formed hydroxide anions can react with monoaromatics via heterolytic hydroxylation [17], which results in the destabilization of the ring structure leading to the ring-opening reactions. Other possible reactions involving hydronium (H<sub>3</sub>O<sup>+</sup>) ions are the dealkylation and substitution by the carbonium mechanism [17], causing the transformation of aromatics into simpler molecules. These complex parallel reactions, together with H<sub>2</sub>O<sub>2</sub>-mediated free radical reactions may contribute to the rapid and efficient destruction of organic pollutants in the homogeneous SCW-Fenton process.

As expected, the degradation performance (%TOC removal) of only SCW treatment is worse than that of Fenton-SCW under the same conditions, which could be ascribed to the absence of H<sub>2</sub>O<sub>2</sub> free radical mechanisms. The oxidative degradation of substituted benzene molecules during SCW treatment might proceed via a heterolytic ring-opening pathway involving electrophilic aromatic substitution of the hydroxyl group and followed by an oxygen attack (HO<sub>2</sub>) radicals [17]. Since the concentration of OH<sup>-</sup> species

in SCW is greater at higher temperatures, the rate and extent of aromatic hydroxylation reaction are enhanced. The thermodynamic activation parameters (i.e.,  $\Delta H^\ddagger$ ,  $\Delta S^\ddagger$ , and  $E_a$ ) for the Fenton-SCW reactions obtained from the Arrhenius and Eyring temperature-rate expressions are presented in Table 2 and the corresponding plots are given in Figure S7. The results indicate that the Fenton-SCW reaction exhibits a lower activation energy ( $E_a$ ), demonstrating that the decomposition of organic pollutants into simpler products is thermodynamically favored at high temperatures. The decreased  $E_a$  may also correlate with the enhanced degradation rate constant in SC.

### 3.3. Heterogeneous SCW-mediated degradation with MIL-88B(Fe)

The TOC removal efficiency of SCW treatment was further investigated in the presence of MIL-88B(Fe) to examine the Fenton-like activity of MOF catalyst in the presence of *in situ* generated OH<sup>-</sup> ions. Due to the strong coordination bonding interactions between Fe(III) and carboxylate linkers based on the Pearson's HSAB principle [34], it is expected that the framework structure of MIL-88B(Fe) possesses high chemical stability in aqueous solutions. As shown in Figure S8, the as-synthesized MOF sample remained stable after soaking in water (pH ~ 6.8) and acid aqueous solution (pH 3) at room temperature overnight without appreciable loss of crystallinity. However, the robustness of MOF catalyst needs to be further assessed under varying temperature conditions of Fenton-SCW process explored in this work, as discussed below.

Prior to the SCW degradation experiments of synthetic wastewater solution, the chemical stability of MIL-88B(Fe) post-SCW treatment for 1 h at temperatures between 100 and 240 °C was examined by XRD analysis. The results demonstrated that the framework integrity of the pristine MOF remained relatively intact following SCW treatment at 100 and 120 °C, where the critical Bragg peaks at  $2\theta = 9.6^\circ$ ,  $16.4^\circ$ , and  $22.2^\circ$  were maintained (Fig. 3a). In the latter case, however, a slightly decreased crystallinity of the treated sample was observed, along with the presence of an impurity phase at  $2\theta = 11.2^\circ$ . On the other hand, the PXRD patterns of the SCW-treated samples at 160, 200, and 240 °C show distinctly different features with the dominant reflections from TPA ligand ( $2\theta = 17.5^\circ$ ,  $25.3^\circ$ , and  $28.2^\circ$ ) and hematite phase ( $\alpha$ -Fe<sub>2</sub>O<sub>3</sub>,  $2\theta = 24.3^\circ$ ,  $33.4^\circ$ ,  $35.8^\circ$ , and  $49.8^\circ$ ), suggesting severe or complete structural degradation of the MOF material. The formation of the hematite-rich phase in the SCW-treated samples at higher temperatures also corresponds well to the observed color change of the resultant solid powder from light brown to a reddish brown (see digital photos in Fig. 3c). SEM analysis revealed that the MIL-88B(Fe) particles hydrothermally treated at 100 and 120 °C

**Table 2**  
Thermodynamic activation parameters of homogeneous Fenton and Fenton-SCW reactions.

System	T, K	$E_a$ , kJ mol <sup>-1</sup>	$\Delta H^\ddagger$ , kJ mol <sup>-1</sup>	$\Delta S^\ddagger$ , J mol <sup>-1</sup> K <sup>-1</sup>
Fenton	303.2	39.2	36.6	-159.7
	308.2			
	313.2			
Fenton-SCW	373.2	21.4	17.8	-228.9
	393.2			
	433.2			
	473.2			
	513.2			

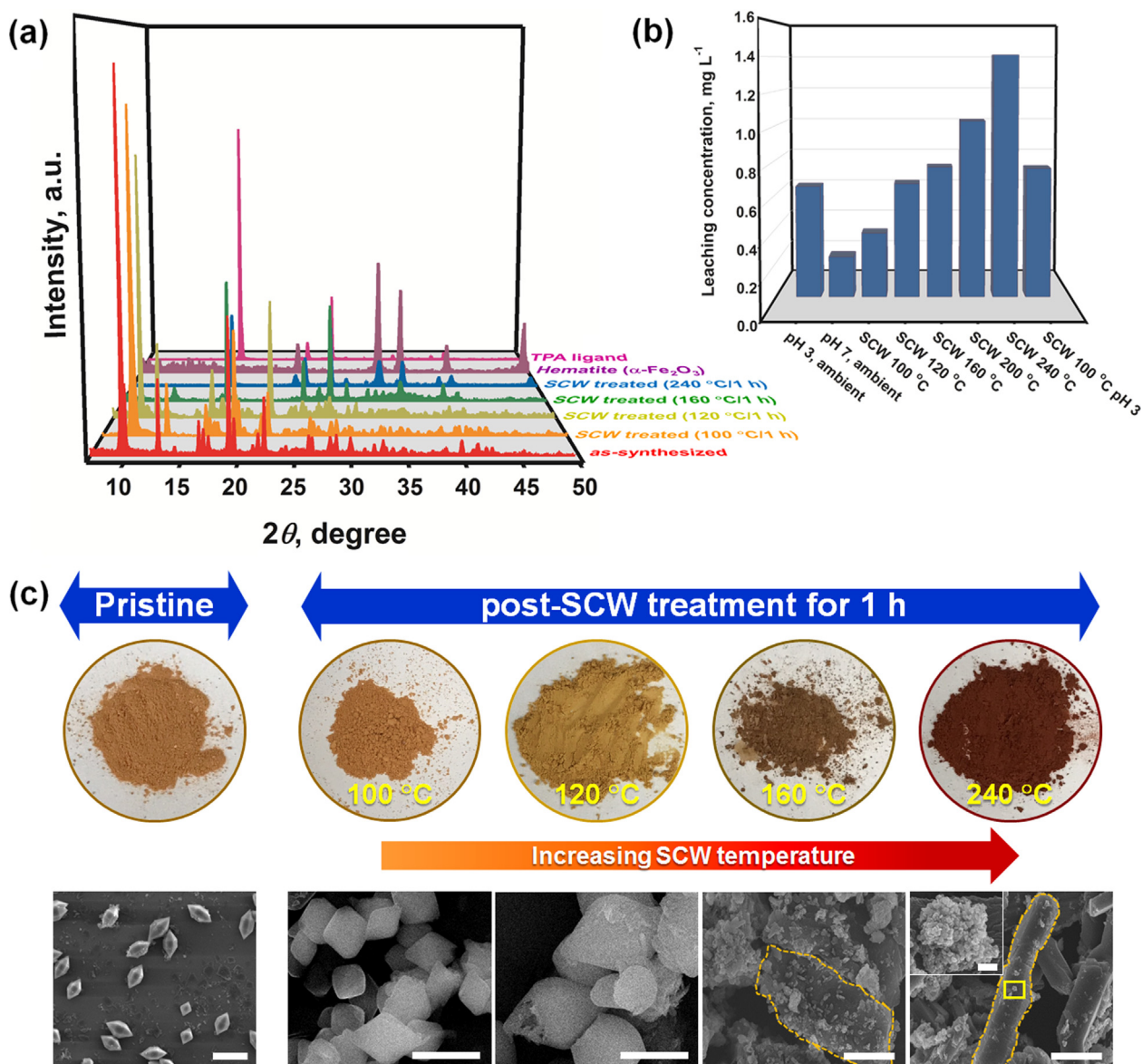


**Fig. 3.** (a) PXRD patterns of the as-synthesized and SCW-treated MIL-88B(Fe) at various temperatures for 1 h. (b) ICP – OES analysis of Fe leaching from MOF catalyst after immersion in water at pH 3 and 7 for 24 h and SCW treatment at various temperatures for 1 h. Reported values are averages of triplicate measurements. (c) Photographs of the pristine crystalline powder of MIL-88B(Fe) and after SCW treatment at various temperatures for 1 h (top row) and their corresponding SEM images (bottom row). The region marked by the orange dashed line represents TPA crystals and the inset shows a magnified image of the yellow-squared area (scale bar: 500 nm). The scale bars correspond to (from left to right) 10 μm, 5 μm, 5 μm, 10 μm, and 10 μm.

maintained their bipyramidal morphology (Fig. 3c, bottom), while those treated at the elevated temperatures (160–240 °C) exhibited slab-like morphology characteristic of TPA crystals with clusters of Fe<sub>2</sub>O<sub>3</sub> nanoparticles deposited on the surface (see inset in the SEM image).

Based on the structural stability evaluation above, we chose 100 °C as the proper reaction temperature for further investigation of Fenton-like catalytic performance of MIL-88B(Fe) in SCW. The result showed that the TOC removal improved slightly from 33.2% in the case of SCW treatment at 100 °C for 60 min to 38.4%

in the presence of 1.5 wt% MIL-88B(Fe). The slightly higher TOC removal in the MIL-88B(Fe)-SCW system can be mainly attributed to the adsorption of model pollutants onto the MOF surface. Thus, it can be implied that the MIL-88B(Fe) shows negligible Fenton-like activity in the SCW medium without the presence of  $\text{H}_2\text{O}_2$ . Further, we analyzed the aqueous solutions post-SCW treatment after removal of MOF particles for Fe leaching by ICP – OES measurement (Fig. 3b). The results showed that the concentrations of dissolved Fe during SCW treatment at 100 and 120 °C for 1 h were determined to be  $0.37 \pm 0.03$  and  $0.67 \pm 0.08 \text{ mg L}^{-1}$ , respectively, which correspond to the <0.1 and ~0.5% leaching of Fe from the catalyst. These leaching concentrations of Fe ions satisfy drinkable water guideline value of 1–3  $\text{mg L}^{-1}$  recommended by WHO. Similarly, the leaching concentrations of Fe ions after 24 h of soaking at room temperature are found to be  $0.65 \pm 0.05$  at pH 3 and  $0.24 \pm 0.03 \text{ mg L}^{-1}$  at pH 7, which are also well below the regulatory standard. An increase in the leaching extent of iron under harsher SCW conditions could be attributed to the more severe hydrolysis reaction that breaks the metal–ligand coordination bonds in MIL-88B(Fe).

### 3.4. SCW-mediated heterogeneous Fenton-like degradation with MIL-88B(Fe)

The treatment performance of heterogeneous Fenton-like process with various MIL-88B(Fe) loadings at a SCW temperature of 100 °C is shown in Fig. 2c. A significant improvement in the degradation efficiency was observed, where the TOC removal percentage reached 92% within 60 min treatment in the presence of 1 wt% catalyst and 9.8 mM  $\text{H}_2\text{O}_2$ . This result indicates that the presence of both MIL-88B(Fe) catalyst and  $\text{H}_2\text{O}_2$  plays a pivotal role in the highly efficient pollutant degradation by the Fenton-like reaction. Increasing the catalyst loading to 1.5 wt% led to only a marginal enhancement in the TOC removal efficiency (95%), while lower dosage of catalyst (0.5 wt%) showed an appreciable decrease in the mineralization efficiency (83% TOC removal). Thus, the optimum catalyst loading was determined to be 1 wt%. It should be noted that no appreciable Fe leaching (~0.2%) from the MOF catalyst was observed during the Fenton-like process under conditions, and thus the contribution of homogeneous Fenton reaction to model organic pollutant degradation caused by leached Fe can be neglected. As shown in Figure S9, an insignificant TOC removal efficiency (<6%) was observed after Fenton-SCW treatment of synthetic wastewater solution at 100 °C for 60 min in the presence of ~0.75  $\text{mg/L Fe}^{3+}$  (simulating Fe leaching) and 9.8 mM  $\text{H}_2\text{O}_2$ , showing good agreement with the above statement. The MIL-88B(Fe) catalyzed Fenton-like SCW system demonstrated superior degradation performance compared to the homogeneous Fenton at room temperature and Fenton-SCW process at elevated temperatures (100–240 °C), as shown in Fig. 2d. Furthermore, as depicted in Figure S10, the residual concentrations of all monoaromatic compounds in the treated wastewater solution that are of concern from a drinking water perspective meet the maximum contaminant level (MCL) established by the U.S. Environmental Protection Agency [44] and the WHO guideline values [48].

To demonstrate the practical feasibility of heterogeneous SCW Fenton-like process, the treatment performance was tested using real environmental samples. In this regard, the real world water samples (i.e., river water, fishpond water, and a wastewater sample collected from a municipal treatment plant, see Text S1 and Table S4 for the characteristics of water samples and details of the pretreatment step) were spiked with PGMEA and monoaromatic compounds at concentrations identical to those in the synthetic wastewater solution and the Fenton-like process was conducted at 100 °C for 60 min in the presence of 1 wt% MIL-88B(Fe) and 19.6 mM  $\text{H}_2\text{O}_2$ . As shown in Fig. 4a, the TOC removal

efficiencies higher than 80% were observed in all spiked real world water samples, demonstrating the great potential of the present approach in practical water and wastewater treatment. It should be noted that the Fenton-like catalytic tests performed in real wastewater matrices indicate a greater degree of catalyst deactivation caused by the blockage of the active sites by dissolved natural organic matter, such as humic acid, thus resulting in decreased degradation efficiency. In this regard, humic acid can bind strongly to Fe(III) surfaces, which would hinder the adsorption of  $\text{H}_2\text{O}_2$  molecules and their decomposition to produce  $\text{HO}^\cdot$  radicals. This explanation is in good agreement with the results of Lindsey and Tarr [21] and Liu et al. [23]. Higher TOC removal efficiencies of  $85.2 \pm 5.8\%$  and  $82.8 \pm 7.2\%$  for the spiked fishpond water and river water, respectively, could be ascribed to lower humic acid concentrations in water samples (see SI, Table S4), which only marginally affect the decomposition efficiency of  $\text{H}_2\text{O}_2$ . The role of dissolved metal ions (e.g., Fe, Cu, and Cr) in the homogeneous Fenton reaction was also investigated (see SI, Figure S9), revealing no appreciable contribution to the overall TOC removal. The reusability of the MOF catalyst in the multiple Fenton-like cycles was evaluated in terms of TOC removal efficiency and chemical stability. Over the course of three consecutive catalytic runs, the TOC removal efficiency slightly decreased from 91.8% to 89.2% (Fig. 4b), thus manifesting good performance of the MOF catalyst for extended operation. The Fenton-like MIL-88B(Fe)-SCW system also shows greater performance degradation than previously reported  $\text{O}_3/\text{H}_2\text{O}_2$  and  $\text{O}_3/\text{UV}$  AOPs [49], as well as catalytic wet oxidation process [26] for treating synthetic wastewater containing PGMEA or monoaromatic compounds (Fig. 4c), thus indicating the great potential of the present approach for an efficient and environmentally benign remediation technology from semiconductor manufacturing effluent.

The TOC removal kinetic profiles of Fenton-like SCW system with MIL-88B(Fe) show a similar trend to that of homogeneous Fenton-SCW system (Fig. 2b). A rapid TOC removal (>60%) occurred in the first 30 min of the reaction for 1 wt% catalyst, which could be ascribed to the highly efficient generation of  $\text{HO}^\cdot$  radicals from the reaction of  $\text{H}_2\text{O}_2$  with open iron coordination sites in MIL-88B(Fe). The kinetic fitting results of the TOC removal efficiency in Figure S5 and Table 3 indicate that all the applied models are able to satisfactorily describe the observed data, where the best fit was obtained with the BMG kinetic model ( $R^2 = 0.995\text{--}0.999$ ). The first- and second-order degradation rate constants (i.e.,  $k_1$  and  $k_2$ ) both increased with increasing catalyst loading, which is associated with the higher availability of catalytic active sites for  $\text{HO}^\cdot$  radical formation. The same trend is observed for the initial rate constant ( $k_{\text{init}}$ ) of Fenton-like reaction from the BMG model fit. Compared to the homogeneous Fenton-SCW reaction catalyzed by the dissolved  $\text{Fe}^{2+}$  ions ( $k_{\text{init}} = 0.343 \text{ min}^{-1}$  at 240 °C), the lower  $k_{\text{init}}$  values ( $k_{\text{init}} = 0.122\text{--}0.296 \text{ min}^{-1}$ ) in the Fenton-like SCW process can be ascribed to the slow rate of hydroxyl radical production through Fe(III)-catalyzed  $\text{H}_2\text{O}_2$  decomposition. The overall degradation rate constants of heterogeneous Fenton-like SCW according to second-order kinetics are at least 1.5 times faster than its homogeneous Fenton-SCW counterpart, reflecting the superior catalytic activity of MIL-88B(Fe). Moreover, the theoretical MOC values range between 114 and 120%, which are higher than that obtained in homogeneous Fenton-SCW at 100 °C ( $\text{MOC}_{\text{cal}} = 76.7\%$ ) under similar conditions.

A proposed mechanism for the Fenton-like catalytic oxidation over MIL-88B(Fe) catalyst is illustrated in Fig. 4d. Surface adsorption of organic pollutants on the bridging linkers of MIL-88B(Fe) takes place before the hydroxyl radical-induced decomposition. In this regard, PGMEA and monoaromatic molecules are adsorbed onto the pore walls of the MIL-88B(Fe) through the carbonyl–aromatic ( $\text{CO}-\pi$ ) [20] and the  $\pi-\pi$  stacking interactions with a

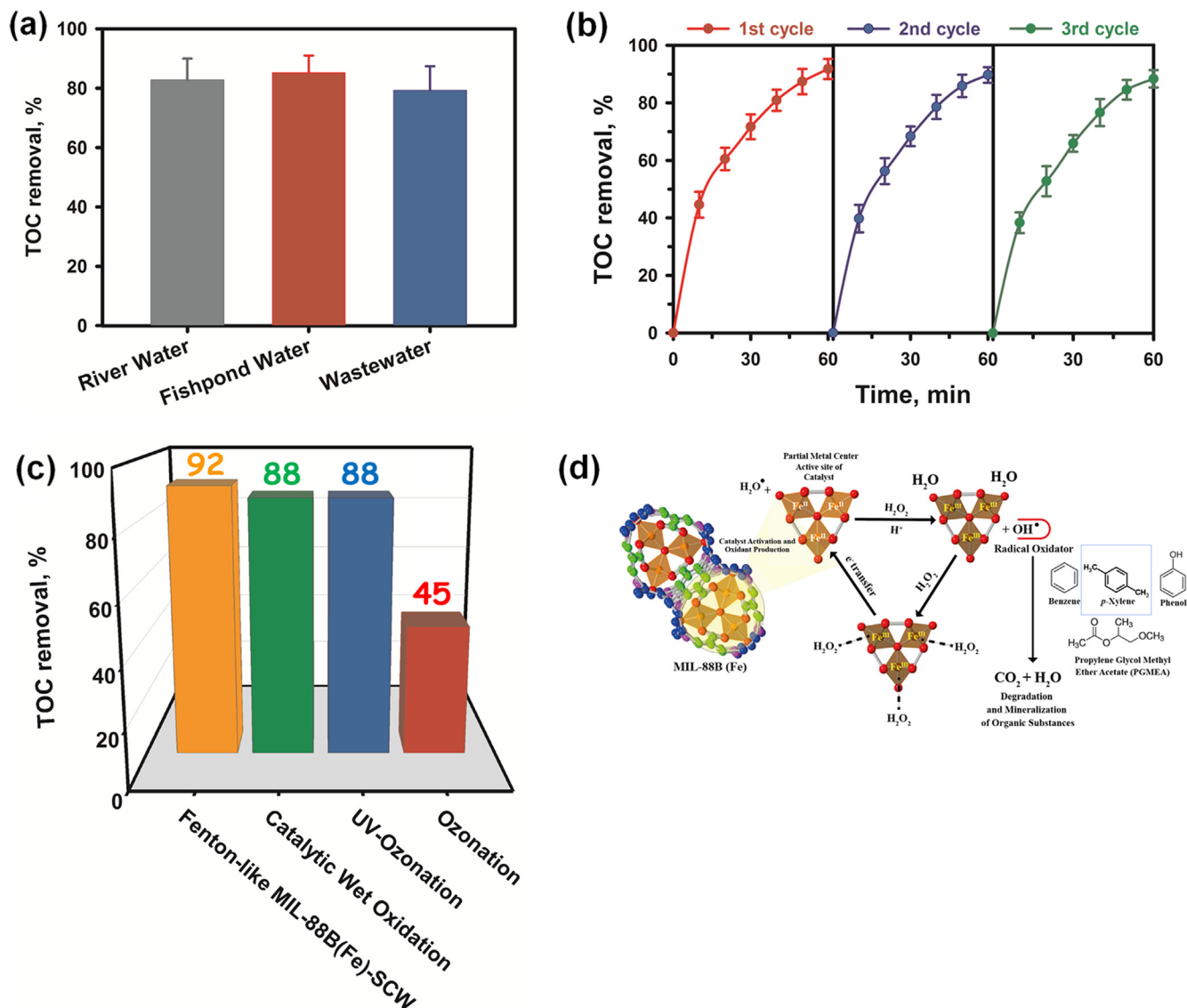


**Fig. 4.** (a) TOC removal efficiency of the heterogeneous Fenton-like treatment of environmental water samples spiked with PGMEA and monoaromatics under SCW conditions of 100 °C for 60 min with 1 wt% MIL-88B(Fe). (b) TOC removal efficiency over three cycles of Fenton-like process in SCW with reused MIL-88B(Fe) catalyst. (c) Comparison of the mineralization efficiency of Fenton-like MIL-88B(Fe)-SCW process with other AOPs, such as ozonation, UV/ozone, and catalytic wet oxidation for the degradation of PGMEA and/or monoaromatic compounds in synthetic wastewater. (d) Proposed Fenton-like reaction mechanism on MIL-88B(Fe) catalyst for oxidative degradation of PGMEA and monoaromatic pollutants.

benzene ring moiety of TPA ligand [33], respectively. In the former case, the CO- $\pi$  aromatic interaction belongs to the attractive ones, due to the electron-withdrawing effect of the carboxyl groups.

Meanwhile, the Lewis acidic Fe<sup>3+</sup> centers with exposed coordination unsaturated sites can readily react with an incoming H<sub>2</sub>O<sub>2</sub> molecule (a strong Lewis base) given their strong affinity for

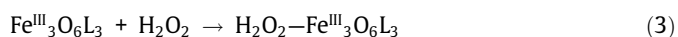
**Table 3**

Fitted kinetic parameters of the first-order, second-order, and BMG models for the TOC removal kinetics in heterogeneous Fenton-like process catalyzed by MIL-88B(Fe) under SCW condition of 100 °C.

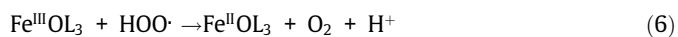
Model <sup>†</sup>	Parameters <sup>‡</sup>	Catalyst loading (wt%)		
		0.5	1.0	1.5
First-order kinetics	$k_1$ (min <sup>-1</sup> )	0.034	0.045	0.055
	$R^2$	0.976	0.985	0.992
Second-order kinetics	$k_2$ (M <sup>-1</sup> min <sup>-1</sup> )	0.061	0.092	0.119
	$R^2$	0.988	0.981	0.975
BMG	$m$ (min)	20.204	15.298	12.912
	$n$	0.881	0.848	0.834
	$k_{\text{init}}$ (min <sup>-1</sup> )	0.049	0.065	0.077
	MOC <sub>cal</sub> (%) <sup>§</sup>	113.5	117.9	119.9
	MOC <sub>exp</sub> (%) <sup>§</sup>	83.5	91.8	95.3
	$R^2$	0.995	0.998	0.999

<sup>†,‡,§</sup> See footnotes in Table 1.

each other [42,51], leading to the formation of iron(III)–H<sub>2</sub>O<sub>2</sub> complex (Eq. (3)). Since the oxidation potential of H<sub>2</sub>O<sub>2</sub> species is larger than the Fe<sup>III</sup>/Fe<sup>II</sup> reduction potential, a facile intermolecular electron transfer occurs between these two species (from H<sub>2</sub>O<sub>2</sub> to the Fe<sup>III</sup> center), leading to the formation of surface Fe(II) species and hydroperoxide radicals (Eq. (4)). The generated surface Fe(II) species subsequently react with H<sub>2</sub>O<sub>2</sub> to generate HO· radicals (Eq. (5)), which proceed via a mechanism analogous to that of ferrous step in the classical Fenton system. Since the adsorbed organic pollutants are located in close vicinity to the Fe<sub>x</sub><sup>II</sup>Fe<sub>1-x</sub><sup>III</sup> metal centers, the HO· radicals can directly attack and oxidize the nearby pollutants, resulting in enhanced mineralization efficiency. The surface Fe(III) species formed during the Fenton-like reaction could further react with hydroperoxide radicals (Eq. (6)) and regenerate surface Fe(II) via a mechanism analogous to that shown in Eq. (2).



where L denotes the TPA bridging ligand {O<sub>2</sub>C–C<sub>6</sub>H<sub>4</sub>–CO<sub>2</sub>}



Several reaction pathways might exist simultaneously during the oxidative degradation of benzene and its substituted derivatives by HO· radicals, which mainly involve electrophilic radical ring addition and radical oxidation of the substituents [1,55]. A recent study by Hara [13] demonstrated that the mineralization of benzene rings into CO<sub>2</sub> in an aqueous system containing H<sub>2</sub>O<sub>2</sub> proceeded via direct oxidation to organic acids, such as glyoxylic (C<sub>2</sub>H<sub>2</sub>O<sub>3</sub>) or oxalic acids (C<sub>2</sub>H<sub>2</sub>O<sub>4</sub>) in a thermodynamically favourable manner. In this regard, the HO· radicals rapidly attack benzene rings and its various intermediates that lead to the benzene-rings excitation and produce CO<sub>2</sub> and H<sub>2</sub>O as the final products (see SI, Figure S11; R<sub>1</sub>). The addition of HO· radicals to the open ring of benzene yields phenol as the intermediate product, which is further oxidized into pyrocatechol and p-benzoquinone (Figure S11; R<sub>2</sub>). In addition, the HO· radicals can induce dehydrogenate and cleavage of benzene rings to produce unsaturated hydrocarbons, followed by subsequent oxidation to simple organic acids (R<sub>3</sub>, R<sub>4</sub>, and R<sub>5</sub>). Some of these organic acids are further decomposed into CO<sub>2</sub> and H<sub>2</sub>O through a Fenton-like process and the rest was decomposed at high temperature through the SCW reaction.

The oxidative decomposition of phenol is begun with the hydroxylation of the aromatic phenol ring by HO· radicals that produce hydroquinone, catechol, and resorcinol [27]. Subsequently, all these intermediate compounds are further oxidized by HO· radicals to maleic acid and finally to simple organic acids, such as oxalic, formic, and acetic acids. Some of these organic acids can readily undergo complete mineralization during the SCW process. The proposed mechanism for the demineralization of phenol is schematically illustrated in Figure S12. The degradation of xylene, cresol, toluene, and PGMEA also produced simple organic acids, which could degrade quickly in Fenton-like conditions and in the SCW process.

#### 4. Conclusions

In summary, we have demonstrated highly efficient degradation of photoresist casting solvent (PGMEA) and monoaromatic compounds in aqueous solution by heterogeneous Fenton-like process using a flexible MIL-88B(Fe) under mild SCW conditions (100 °C; 60 min). The resulting bipyramidal MOF microcrystals exhibit mesoporous structure, as well as good framework stability

upon SCW treatment at 100 °C. The incorporation of MIL-88B(Fe) into the Fenton-like SCW system can achieve high-efficiency mineralization of synthetic wastewater solution with ~92% TOC removal efficiency, which shows superior performance compared to the homogeneous Fenton and Fenton-SCW processes with 54% and 60% removal efficiency, respectively. The TOC removal kinetic profiles in the SCW-mediated homogeneous Fenton and heterogeneous Fenton-like systems are found to be well-fitted to the BMG model. Furthermore, the practical feasibility of this approach has been demonstrated to degrade the target contaminants in various real world water samples with satisfactory mineralization efficiency. Overall, the heterogeneous Fenton-like process employing a reusable Fe-based breathing MOF catalyst under mild SCW conditions represents an attractive environmentally friendly strategy for highly efficient degradation of recalcitrant organic pollutants in semiconductor manufacturing effluents and other complex wastewater matrices.

#### CRedit authorship contribution statement

**Felycia Edi Soetaredjo:** Conceptualization, Supervision, Funding acquisition. **Shella Permatasari Santoso:** Methodology, Supervision, Formal analysis. **Valentino Bervia Lunardi:** Investigation, Data curation, Writing – original draft. **Alfin Kurniawan:** Conceptualization, Visualization, Writing – review & editing. **Hardy Shuwanto:** Investigation, Validation. **Jenni Lie:** Investigation, Validation. **Kuncoro Foe:** Project administration. **Wenny Irawaty:** Formal analysis. **Maria Yuliana:** Formal analysis, Data curation. **Jindrayani Nyoo Putro:** Formal analysis, Validation. **Artik Elisa Angkawijaya:** Resources. **Yi-Hsu Ju:** Resources. **Suryadi Ismadji:** Resources, Project administration, Writing – original draft.

#### Declaration of Competing Interest

The authors declare that they have no known competing financial interests or personal relationships that could have appeared to influence the work reported in this paper.

#### Acknowledgements

This work was financially supported by the Directorate of Research and Community Service, Deputy for Research and Development Strengthening, Ministry of Research and Technology/National Agency for Research and Innovation, Republic of Indonesia, through contract number 150A/WM01.5/N/2021.

#### Appendix A. Supplementary material

Supplementary data to this article can be found online at <https://doi.org/10.1016/j.molliq.2021.117989>.

#### References

- [1] M. Anbar, D. Meyerstein, P. Neta, The reactivity of aromatic compounds toward hydroxyl radicals, *J. Phys. Chem.* 70 (1966) 2660–2662.
- [2] M.G. Antoniou, C. Zhao, K.E. O'Shea, G. Zhang, D.D. Dionysiou, C. Zhao, C. Han, M.N. Nadagouda, H. Choi, T. Fotiou, T.M. Triantis, A. Hiskia, Photocatalytic degradation of organic contaminants in water: Process optimization and degradation pathways, in: D.D. Dionysiou, G.L. Puma, J. Ye, J. Schneider, D. Bahnemann (Eds.), *Photocatalysis: Applications*, Royal Society of Chemistry, 2016, pp. 1–34.
- [3] A. Babuponnusami, K. Muthukumar, Advanced oxidation of phenol: A comparison between Fenton, electro-Fenton, sono-electro-Fenton and photo-electro-Fenton processes, *Chem. Eng. J.* 183 (2012) 1–9.
- [4] L.L.E. Bayon, F.C. Ballesteros Jr., S. Garcia-Segura, M.-C. Lu, Water reuse nexus with resource recovery: On the fluidized-bed homogeneous crystallization of copper and phosphate from semiconductor wastewater, *J. Clean. Prod.* 236 (2019) 117705.

- [5] M.A. Behnajady, N. Modirshahla, F. Ghanbary, A kinetic model for the decolorization of C.I. acid yellow 23 by Fenton process, *J. Hazard. Mater.* 148 (2007) 98–102.
- [6] R. Chepesiuk, Where the chips fall: environmental health in the semiconductor industry, *Environ. Health Perspect.* 107 (1999) A452–A457.
- [7] E. Croiset, S.F. Rice, R.G. Hanush, Hydrogen peroxide decomposition in supercritical water, *AIChE J.* 43 (1997) 2343–2352.
- [8] C.K. Duesterberg, S.E. Mylon, T.D. Waite, pH effects on iron-catalyzed oxidation using Fenton's reagent, *Environ. Sci. Technol.* 42 (2008) 8522–8527.
- [9] A. El-Ghenymy, J.A. Garrido, F. Centellas, C. Arias, P.L. Cabot, R.M. Rodríguez, E. Brillas, Electro-Fenton and photoelectron-Fenton degradation of sulfanilic acid using a boron-doped diamond anode and an air diffusion cathode, *J. Phys. Chem. A* 116 (2012) 3404–3412.
- [10] C. Gao, S. Chen, X. Quan, H. Yu, Y. Zhang, Enhanced Fenton-like catalysis by iron-based metal organic frameworks for degradation of organic pollutants, *J. Catal.* 356 (2017) 125–132.
- [11] F. Gunawan, A. Kurniawan, I. Gunawan, Y.-H. Ju, A. Ayucitra, F.E. Soetaredjo, S. Ismadji, Synthesis of biodiesel from vegetable oils wastewater sludge by *in-situ* subcritical methanol transesterification: Process evaluation and optimization, *Biomass Bioenergy* 69 (2014) 28–38.
- [12] K.I. Hadjiivanov, D.A. Panayotov, M.H. Mihaylov, E.Z. Ivanova, K.K. Chakarova, S.M. Andonova, N.L. Drenchev, Power of infrared and Raman spectroscopies to characterize metal-organic frameworks and investigate their interaction with guest molecules, *Chem. Rev.* 121 (2021) 1286–1424.
- [13] J. Hara, Oxidative degradation of benzene rings using iron sulfide activated by hydrogen peroxide/ozone, *Chemosphere* 189 (2017) 382–389.
- [14] P. Horcajada, F. Salles, S. Wuttke, T. Devic, D. Heurtaux, G. Maurin, A. Vimont, M. Daturi, O. David, E. Magnier, N. Stock, Y. Filinchuk, D. Popov, C. Riekkel, G. Férey, C. Serre, How linker's modification controls swelling properties of highly flexible iron(III) dicarboxylates MIL-88, *J. Am. Chem. Soc.* 133 (2011) 17839–17847.
- [15] L.-C. Hsu, C.-Y. Huang, Y.-H. Chuang, H.-W. Chen, Y.-T. Chan, H.Y. Teah, T.-Y. Chen, C.-F. Chang, Y.-T. Liu, Y.-M. Tzou, Accumulation of heavy metals and trace elements in fluvial sediments received effluents from traditional and semiconductor industries, *Sci. Rep.* 6 (2016) 34250.
- [16] S.-C. Hsu, H.-L. Hsieh, C.-P. Chen, C.-M. Tseng, S.-C. Huang, C.-H. Huang, Y.-T. Huang, V. Radashevsky, S.-H. Lin, Tungsten and other heavy metal contamination in aquatic environments receiving wastewater from semiconductor manufacturing, *J. Hazard. Mater.* 189, 193–202. Huang, S.-Z., Wu, K.-Y., 2019. Health risk assessment of photoresists used in an optoelectronic semiconductor factory, *Risk Anal.* 39 (2011) 2625–2639.
- [17] Y.-L. Kim, J.-D. Kim, J.S. Lim, Y.-W. Lee, S.-C. Yi, Reaction pathway and kinetics for uncatalyzed partial oxidation of *p*-xylene in sub- and supercritical water, *Ind. Eng. Chem. Res.* 41 (2002) 5576–5583.
- [18] A. Kruse, A. Gawlik, Biomass conversion in water at 330–410 °C and 30–50 MPa. Identification of key compounds for indicating different chemical reaction pathways, *Ind. Eng. Chem. Res.* 42 (2003) 267–279.
- [19] A. Kurniawan, C. Effendi, L.K. Ong, Y.-H. Ju, C.X. Lin, S. Ismadji, Novel, integrated biorefinery approach of *Ceiba pentandra* (kapok) seed and its secondary waste, *ACS Sustain. Chem. Eng.* 1 (2013) 473–480.
- [20] P. Li, E.C. Vik, J.M. Maier, I. Karki, S.M.S. Strickland, J.M. Umana, M.D. Smith, P.J. Pellechia, K.D. Shimizu, Electrostatically driven CO- $\pi$  aromatic interactions, *J. Am. Chem. Soc.* 141 (2019) 12513–12517.
- [21] M.E. Lindsey, M.A. Tarr, Inhibition of hydroxyl radical reaction with aromatics by dissolved natural organic matter, *Environ. Sci. Technol.* 34 (2000) 444–449.
- [22] Z. Lionet, T.-H. Kim, Y. Horiuchi, S.W. Lee, M. Matsuoka, Linker engineering of iron-based MOFs for efficient visible-light-driven water oxidation reaction, *J. Phys. Chem. C* 123 (2019) 27501–27508.
- [23] B. Liu, Z. Liu, P. Yu, S. Pan, Y. Xu, Y. Sun, S.-Y. Pan, Y. Yu, H. Zheng, Enhanced removal of tris(2-chloroethyl) phosphate using a resin-based nanocomposite hydrated iron oxide through a Fenton-like process: Capacity evaluation and pathways, *Water Res.* 175 (2020) 115655.
- [24] H. Lu, Z. Zhu, H. Zhang, J. Zhu, Y. Qiu, L. Zhu, S. Kuppers, Fenton-like catalysis and oxidation/adsorption performances of acetaminophen and arsenic pollutants in water on a multimetal Cu–Zn–Fe-LDH, *ACS Appl. Mater. Interfaces* 8 (2016) 25343–25352.
- [25] M. Ma, A. Bétard, I. Weber, N.S. Al-Hokbany, R.A. Fischer, N. Metzler-Nolte, Iron-based metal-organic frameworks MIL-88B and NH<sub>2</sub>-MIL-88B: High quality microwave synthesis and solvent-induced lattice “breathing”, *Cryst. Growth Des.* 13 (2013) 2286–2291.
- [26] R. Mohite, A. Garg, Performance of supported copper catalysts for oxidative degradation of phenolics in aqueous medium: Optimization of reaction conditions, kinetics, catalyst stability, characterization, and reusability, *Ind. Eng. Chem. Res.* 59 (2020) 12986–12998.
- [27] E. Mousset, L. Frunzo, G. Esposito, E.D. van Hullebusch, N. Oturan, M.A. Oturan, A complete phenol oxidation pathway obtained during electro-Fenton treatment and validated by a kinetic model study, *Appl. Catal. B-Environ.* 180 (2016) 189–198.
- [28] M.K.S. Nascimento, S. Loureiro, M.R. dos Reis Souza, M. da Rosa Alexandre, J. Nilin, Toxicity of a mixture of monoaromatic hydrocarbons (BTX) to a tropical marine microcrustacean, *Mar. Pollut. Bull.* 156 (2020) 111272.
- [29] S. Navalon, M. de Miguel, R. Martin, M. Alvaro, H. Garcia, Enhancement of the catalytic activity of supported gold nanoparticles for the Fenton reaction by light, *J. Am. Chem. Soc.* 133 (2011) 2218–2226.
- [30] R. Nivetha, P. Kollu, K. Chandar, S. Pitchaimuthu, S.K. Jeong, A.N. Grace, Role of MIL-53 (Fe)/hydrated–dehydrated MOF catalyst for electrochemical hydrogen evolution reaction (HER) in alkaline medium and photocatalysis, *RSC Adv.* 9 (2019) 3215–3223.
- [31] Y. Orita, M. Akizuki, Y. Oshima, Dual-stage method using supercritical and subcritical water for precise control of size and distribution of CeO<sub>2</sub> nanoparticles, *Ind. Eng. Chem. Res.* 59 (2020) 3035–3043.
- [32] S.-H. Park, J.-A. Shin, H.-H. Park, G.Y. Yi, K.-J. Chung, H.-D. Park, K.-B. Kim, I.-S. Lee, Exposure to volatile organic compounds and possibility of exposure to by-product volatile organic compounds in photolithography processes in semiconductor manufacturing factories, *Safety Health Work* 2 (2011) 210–217.
- [33] D.V. Patil, P.B.S. Rallapalli, G.P. Dangl, R.J. Tayade, R.S. Somani, H.C. Bajaj, MIL-53(Al): An efficient adsorbent for the removal of nitrobenzene from aqueous solutions, *Ind. Eng. Chem. Res.* 50 (2011) 10516–10524.
- [34] R.G. Pearson, Hard and soft acids and bases, HSAB, part 1: Fundamental principles, *J. Chem. Educ.* 45 (1968) 581.
- [35] L. Peng, C.-T. Hung, S. Wang, X. Zhang, X. Zhu, Z. Zhao, C. Wang, Y. Tang, W. Li, D. Zhao, Versatile nanoemulsion assembly approach to synthesize functional mesoporous carbon nanospheres with tunable pore sizes and architectures, *J. Am. Chem. Soc.* 141 (2019) 7073–7080.
- [36] P.E. Savage, Organic chemical reactions in supercritical water, *Chem. Rev.* 99 (1999) 603–621.
- [37] Semiconductor Market Report: Trends, Forecast and Competitive Analysis. <https://www.lucintel.com/semiconductor-market.aspx> (accessed 11 January 2021).
- [38] C. Serre, C. Mellot-Draznieks, S. Surblé, N. Audebrand, Y. Filinchuk, G. Férey, Role of solvent-host interactions that lead to very large swelling of hybrid frameworks, *Science* 315 (2007) 1828–1831.
- [39] Y. Shinozawa, D. Heggo, S. Ookawara, S. Yoshikawa, Photo-Fenton degradation of carbofuran in helical tube microreactor and kinetic modeling, *Ind. Eng. Chem. Res.* 59 (2020) 3811–3819.
- [40] C.A. Staples, J.W. Davis, An examination of the physical properties, fate, ecotoxicity and potential environmental risks for a series of propylene glycol ethers, *Chemosphere* 49 (2002) 61–73.
- [41] S. Tadrent, D. Luart, O. Bals, A. Khelifa, R. Luque, C. Len, Metal-free reduction of nitrobenzene to aniline in subcritical water, *J. Org. Chem.* 83 (2018) 7431–7437.
- [42] J. Tang, J. Wang, Metal organic framework with coordinatively unsaturated sites as efficient Fenton-like catalyst for enhanced degradation of sulfamethazine, *Environ. Sci. Technol.* 52 (2018) 5367–5377.
- [43] M. Thommes, K. Kaneko, A.V. Neimark, J.P. Olivier, F. Rodriguez-Reinoso, J. Rouquerol, K.S.W. Sing, Physiosorption of gases, with special reference to the evaluation of surface area and pore size distribution (IUPAC Technical Report), *Pure Appl. Chem.* 87 (2015) 1051–1069.
- [44] U.S. EPA, 2018 Edition of the Drinking Water Standards and Health Advisories, U.S. Environmental Protection Agency Report EPA 822-F-18-001, Office of Water, Washington, DC, 2018.
- [45] D. Wang, R. Huang, W. Liu, D. Sun, Z. Li, Fe-based MOFs for photocatalytic CO<sub>2</sub> reduction: Role of coordination unsaturated sites and dual excitation pathways, *ACS Catal.* 4 (2014) 4254–4260.
- [46] D. Wang, M. Wang, Z. Li, Fe-based metal-organic frameworks for highly selective photocatalytic benzene hydroxylation to phenol, *ACS Catal.* 5 (2015) 6852–6857.
- [47] X. Wang, Q. Wang, C. Ye, X. Dong, T. Qiu, Feasibility study of reactive distillation for the production of propylene glycol monomethyl ether acetate through transesterification, *Ind. Eng. Chem. Res.* 56 (2017) 7149–7159.
- [48] World Health Organization, Guidelines for Drinking-water Quality, fourth ed. incorporating the first addendum, Geneva, Switzerland, 2017.
- [49] J.J. Wu, M. Muruganandham, L.T. Chang, S.H. Chen, Oxidation of propylene glycol methyl ether acetate using ozone-based advanced oxidation processes, *Ozone. Sci. Eng.* 30 (2008) 332–338.
- [50] L. Xu, J. Wang, Magnetic nanoscaled Fe<sub>3</sub>O<sub>4</sub>/CeO<sub>2</sub> composite as an efficient Fenton-like heterogeneous catalyst for degradation of 4-chlorophenol, *Environ. Sci. Technol.* 46 (2012) 10145–10153.
- [51] X.-J. Yang, X.-M. Xu, J. Xu, Y.-F. Han, Iron oxychloride (FeOCl): An efficient Fenton-like catalyst for producing hydroxyl radicals in degradation of organic contaminants, *J. Am. Chem. Soc.* 135 (2013) 16058–16061.
- [52] Y. Yin, L. Shi, W. Li, X. Li, H. Wu, Z. Ao, W. Tian, S. Liu, S. Wang, H. Sun, Boosting Fenton-like reactions via single atom Fe catalysis, *Environ. Sci. Technol.* 53 (2019) 11391–11400.
- [53] E.T. Zellers, R. Sulewski, Glove permeation by propylene glycol monomethyl ether acetate – A photoresist solvent used in semiconductor device processing, *Appl. Occup. Environ. Hyg.* 7 (1992) 392–397.
- [54] M. Zhang, Z. Zhang, S. Liu, Y. Peng, J. Chen, S.Y. Ki, Ultrasound-assisted electrochemical treatment for phenolic wastewater, *Ultrason. Sonochem.* 65 (2020) 105058.
- [55] N. Zhang, I. Geronimo, P. Paneth, J. Schindelka, T. Schaefer, H. Herrmann, C. Vogt, H.H. Richnow, Analyzing sites of OH radical attack (ring vs. side chain) in oxidation of substituted benzenes via dual stable isotope analysis ( $\delta^{13}\text{C}$  and  $\delta^2\text{H}$ ), *Sci. Total. Environ.* 542 (2016) 484–494.
- [56] S.-W. Zou, C.-W. How, J.P. Chen, Photocatalytic treatment of wastewater contaminated with organic waste and copper ions from the semiconductor industry, *Ind. Eng. Chem. Res.* 46 (2007) 6566–6571.